Journal of the Optical Society of America B
OPTICAL PHYSICS

Metal-nanoparticle arrays on a magnetic garnet film for tunable plasmon-enhanced Faraday rotation

Evangelos Almpanis,[1,*] Petros-Andreas Pantazopoulos,[2] Nikolaos Papanikolaou,[3] Vassilios Yannopapas,[1] and Nikolaos Stefanou[2]

[1]Department of Physics, National Technical University of Athens, GR-157 80 Athens, Greece
[2]Department of Solid State Physics, National and Kapodistrian University of Athens, University Campus, GR-157 84 Athens, Greece
[3]Institute of Nanoscience and Nanotechnology, NCSR "Demokritos," Patriarchou Gregoriou and Neapoleos Str., Ag. Paraskevi, GR-153 10 Athens, Greece
*Corresponding author: ealmpanis@gmail.com

Received 25 August 2016; revised 25 October 2016; accepted 31 October 2016; posted 2 November 2016 (Doc. ID 274537); published 28 November 2016

We developed an extension of the layer-multiple-scattering method to photonic crystals comprising homogeneous layers of magneto-optical materials. The applicability of the method is demonstrated on a specific architecture of a magnetic garnet thin film coated with a square array of silver nanodisks, supported by a silica substrate. It is shown that enhanced Faraday rotation, driven by hybrid particle plasmon-film quasi-guided collective modes, can be achieved within selected regions of frequency, which can be tuned by properly choosing the geometric and material parameters involved. The results are analyzed in conjunction with numerical simulations by the finite-element method and a consistent interpretation of the underlying physics is provided. Our extended layer-multiple-scattering computational methodology provides a versatile framework for fast and accurate full electrodynamic calculations of magneto-optical structures, enabling physical insight.

OCIS codes: (350.4238) Nanophotonics and photonic crystals; (290.4210) Multiple scattering; (250.5403) Plasmonics; (160.3820) Magneto-optical materials.

https://doi.org/10.1364/JOSAB.33.002609

1. INTRODUCTION

Appropriately structured dielectric magnetic films provide impressive opportunities for tailoring the magneto-optical (MO) interaction and consequent phenomena, such as the Faraday effect. In the Faraday configuration, an external static magnetic field is applied perpendicular to the film, so that the film becomes magnetically saturated, causing a rotation in the polarization vector of normally incident linearly polarized light as it propagates through the structure. The polarization rotation angle of the transmitted wave is called the Faraday rotation angle. Such structures are very useful in the realization of optical isolation [1,2], magnetically induced polarization control, and the use of the polarization state as an information carrier. Nanostructuring allows one to overcome the problem of rather weak MO interaction in a bare thin magnetic film by enhancing the electromagnetic (EM) field in the active magnetic region and thus achieving Faraday rotation angles similar to those obtained by much thicker magnetic films. For this purpose, Kato *et al.* [3] studied a bismuth-substituted yttrium iron garnet (Bi:YIG) thin film sandwiched between two dielectric Bragg mirrors, where the confinement of the EM field inside the magnetic film, which operates as a photonic cavity, enhances the Faraday rotation angle almost 10 times compared to that of the bare Bi:YIG film, reaching values ranging from 1° to 3° for a 150 nm thick Bi:YIG film. However, even this all-dielectric structure exhibits considerable losses and the measured transmittance at the resonance frequency does not exceed 15%. Moreover, the structure is rather bulky and thus it is not suitable for highly integrable MO devices.

As an alternative to the above design, the combination of plasmonic and MO functionalities in thin-film architectures has also been proposed [4–6]. Surface plasmons are EM waves coupled to collective oscillations of the electrons at an interface between two media with permittivities of opposite sign, typically a dielectric and a metal. In particular, localized surface plasmon (LSP) modes, also called particle plasmons, are plasma oscillations occurring at the surface of a finite nano-object, e.g., a sphere or a disk. One of the most salient features of metallic

nanostructures supporting surface plasmons is their ability to localize light in subwavelengh volumes resulting in huge values of the local field [7]. If optically active materials are placed in the vicinity of LSP-supporting nano-objects, their optical response can be strongly affected by the ensuing enhancement of the local field. A direct application of this effect is the modification of the MO response of magnetic materials via different enhancement mechanisms, such as enhanced effective particle polarizability [8–15], effective increase of the optical path [16–18], and tailored wave dispersion [19–23].

Following this strategy, in a setup appropriate for enhancing Faraday rotation, a magnetic garnet film was sandwiched between a perforated metallic film and a glass substrate in geometries demonstrating the phenomenon of extraordinary optical transmission [24–29]. In these geometries, the Faraday rotation maximum appears at a peak in the transmittance that typically reaches 30%–40%, while, at the same time, an up to 10-fold Faraday rotation enhancement in absolute value can be achieved, depending on the operating wavelength region [24–26]. Using a trilayer structure, with a dielectric spacer between a Bi:YIG slab and a perforated metallic film, the transmittance was shown to reach 46% at the peak of the Faraday rotation angle, $\phi = 2.58°$, in the infrared [27], though recent attempts with a similar configuration in the visible spectrum reported 50% transmittance but the Faraday rotation angle, for a 100 nm thick Bi:YIG film, did not exceed 0.35° [28]. A resonance with high transmittance (63%) but still a moderate Faraday rotation angle (−0.74°) at infrared frequencies has been demonstrated in a bilayer structure consisting of a perforated metallic film with circular annular arrays on top of a Bi:YIG film [29]. Moreover, in this structure, another resonance that further enhances the Faraday rotation angle, which reaches almost 3.5°, is also present. This resonance, however, comes with a cost in the transmittance, which is significantly reduced to below 1%. It is a general issue that the significant enhancement of the Faraday rotation angle in magnetoplasmonic structures comes with a cost in the transmitted field, especially at visible frequencies. This is because the desirable property of field localization and enhancement associated with plasmons is intimately connected with absorption losses. It has also been reported that, in arrays of Au nanodisks buried in a Bi:YIG film, the LSP resonance enhances the Faraday rotation by almost a factor of 5 but, again, dissipative losses reduce the corresponding transmittance, which ranges from 5% to 10% [30,31]. We note that, in such configurations of metallic nanoparticles or nanogratings, the Faraday rotation peak corresponds to a dip rather than a peak in the transmittance.

The excitation of hybrid plasmonic-quasi-guided modes of a nanopatterned magnetic garnet film has also been proposed as a possible way to obtain a balance between transmittance and Faraday rotation enhancement [32,33]. A periodic arrangement of Au nanogratings on top of a Bi:YIG film yields an almost 10-fold enhancement of Faraday rotation [32] with a corresponding transmittance 36% for an incident plane wave polarized perpendicular to the grating. Nevertheless, the grating geometry renders the structure polarization-sensitive and the wavelength of the hybrid resonance is not easily tunable. Alternatively, a two-dimensional periodic array of metallic nanoparticles could also provide a means to excite guided modes of the garnet film, hybridized with LSP resonances, offering a fully tunable setup for the enhancement of the polarization rotation and control of the phase of an incident plane wave. In a square array of symmetrical nanoparticles, the two polarization states are degenerate for normal incidence, leading to efficient coupling with the guided modes of the magnetic garnet film, which in turn would increase the rate of polarization conversion. Such a MO metasurface, consisting of a square array of Ag nanodisks on top of a thin Bi:YIG film deposited on a silica substrate, will be investigated in the present paper. Due to periodicity, the guided modes of the film can couple to external radiation, and characteristic Fano-type signatures are present in the transmission spectrum, even for normally incident light. On the other hand, LSP resonances, supported by the metallic nanoparticles, have the ability to enhance and confine light in subwavelength dimensions. The interaction of LSP resonances with guided modes of the film can lead to hybrid modes of mixed character, allowing for higher MO interaction and transmittance, due to the strong field localization in the magnetic film and the significantly lower losses compared to common plasmonic resonances.

By understanding the underlying physics, which involves the coupling between the LSP and the waveguide modes of the magnetic film, one will be able to design structures with the desirable figure of merit, which expresses the trade-off between transmittance and Faraday rotation angle. These structures are fully tunable with the geometry and, depending on the materials, large Faraday rotation angles can be achieved. Of course, such an optimization process requires large-scale systematic and rigorous calculations, which, in the present paper, are carried out using the layer-multiple-scattering (LMS) method [34–36] that we properly extend so as to treat structures comprising layers of magnetic materials. So far, the method could handle structures of magnetic particles [37–39] but not magnetic films. Contrary to other time-consuming methods, LMS constitutes a fast and accurate computational methodology that is ideally suited for the structures under consideration. The efficiency of the method for nonmagnetic photonic structures was recently demonstrated in a comparison with the widely used commercial finite-element solver implemented in the COMSOL Multiphysics package [40]. For the same level of accuracy (fully converged calculations), the LMS method is almost two orders of magnitude faster than the finite-element method for three-dimensional systems with anisotropy and nonspherical scatterers. The combination of two different optimal basis sets, spherical waves for in-plane (interparticle) and plane waves for interlayer multiple scattering, is one of the key characteristics to which LMS owes its efficiency. Indeed, this combination leads to matrices of relatively small size and significantly reduces the computational cost for matrix manipulations, compared to other methods that solve the scattering problem, e.g., in a plane wave basis, such as the scattering-matrix [41,42] and the rigorous-coupled-wave-analysis methods [21,43].

2. COMPUTATIONAL METHOD

Our calculations are carried out by the LMS method [34–36], which we extended so as to treat structures that comprise

homogeneous layers of optically anisotropic materials described by a relative electric permittivity tensor of the general form

$$\varepsilon = \begin{pmatrix} \varepsilon_{xx} & \varepsilon_{xy} & \varepsilon_{xz} \\ \varepsilon_{yx} & \varepsilon_{yy} & \varepsilon_{yz} \\ \varepsilon_{zx} & \varepsilon_{zy} & \varepsilon_{zz} \end{pmatrix} \tag{1}$$

and a scalar relative magnetic permeability μ. In such an infinite birefringent medium, Maxwell's equations accept monochromatic plane wave solutions of angular frequency ω and wave vector $\mathbf{q}$, with the electric field amplitude components satisfying the following homogeneous system of linear equations [44]:

$$\begin{pmatrix} \omega^2\mu\varepsilon_{xx}\varepsilon_0\mu_0 - q_y^2 - q_z^2 & \omega^2\mu\varepsilon_{xy}\varepsilon_0\mu_0 + q_xq_y & \omega^2\mu\varepsilon_{xz}\varepsilon_0\mu_0 + q_xq_z \\ \omega^2\mu\varepsilon_{yx}\varepsilon_0\mu_0 + q_xq_y & \omega^2\mu\varepsilon_{yy}\varepsilon_0\mu_0 - q_x^2 - q_z^2 & \omega^2\mu\varepsilon_{yz}\varepsilon_0\mu_0 + q_yq_z \\ \omega^2\mu\varepsilon_{zx}\varepsilon_0\mu_0 + q_xq_z & \omega^2\mu\varepsilon_{zy}\varepsilon_0\mu_0 + q_yq_z & \omega^2\mu\varepsilon_{zz}\varepsilon_0\mu_0 - q_y^2 - q_x^2 \end{pmatrix} \begin{pmatrix} E_{0x} \\ E_{0y} \\ E_{0z} \end{pmatrix} = 0, \tag{2}$$

where ε_0 and μ_0 are the electric permittivity and magnetic permeability of vacuum, respectively. Also in the spirit of the LMS method, considering ω and the components of the wave vector parallel to the interfaces of a stratified composite structure, $\mathbf{q}_\parallel = (q_x, q_y)$, as given quantites, the allowed values of q_z and the corresponding electric field polarization unit vectors, $\hat{\mathbf{e}}$, where $\mathbf{E}_0 = E_0\hat{\mathbf{e}}$, can be most efficiently determined if we cast Eq. (2) in the form of a quadratic eigenvalue problem

$$(q_z^2\mathbf{M} + q_z\mathbf{C} + \mathbf{K})\hat{\mathbf{e}} = 0, \tag{3}$$

where

$$\mathbf{M} = \begin{pmatrix} -1 & 0 & 0 \\ 0 & -1 & 0 \\ 0 & 0 & 0 \end{pmatrix}, \qquad \mathbf{C} = \begin{pmatrix} 0 & 0 & q_x \\ 0 & 0 & q_y \\ q_x & q_y & 0 \end{pmatrix},$$

$$\mathbf{K} = \begin{pmatrix} \omega^2\mu\varepsilon_{xx}\varepsilon_0\mu_0 - q_y^2 & \omega^2\mu\varepsilon_{xy}\varepsilon_0\mu_0 + q_xq_y & \omega^2\mu\varepsilon_{xz}\varepsilon_0\mu_0 \\ \omega^2\mu\varepsilon_{yx}\varepsilon_0\mu_0 + q_xq_y & \omega^2\mu\varepsilon_{yy}\varepsilon_0\mu_0 - q_x^2 & \omega^2\mu\varepsilon_{yz}\varepsilon_0\mu_0 \\ \omega^2\mu\varepsilon_{zx}\varepsilon_0\mu_0 & \omega^2\mu\varepsilon_{zy}\varepsilon_0\mu_0 & \omega^2\mu\varepsilon_{zz}\varepsilon_0\mu_0 - q_y^2 - q_x^2 \end{pmatrix}. \tag{4}$$

We note that only four out of the six eigenvalues q_z are finite, the other two being infinite since $\mathbf{M}$ is singular and the characteristic polynomial, $\det[q_z^2\mathbf{M} + q_z\mathbf{C} + \mathbf{K}]$, is of fourth degree [45]. Equation (3) is solved numerically by the algorithm of Hammarling *et al.* [46]. We denote the four physically acceptable eigenvalues by $q_{z;p}^s$, where $s = +(-)$ describes waves propagating or evanescent in the positive (negative) z direction and $p = 1, 2$ labels two linearly independent polarization eigenmodes. The electric and magnetic field components of these waves, of wave vector $\mathbf{q}_p^s = \mathbf{q}_\parallel + q_{z;p}^s\hat{\mathbf{z}}$ and polarization eigenvector $\hat{\mathbf{e}}(\mathbf{q}_p^s)$, are given by

$$\mathbf{E}(\mathbf{r}, t) = \mathrm{Re}\{E_0\ \exp[i(\mathbf{q}_p^s \cdot \mathbf{r} - \omega t)]\hat{\mathbf{e}}(\mathbf{q}_p^s)\},$$

$$\mathbf{H}(\mathbf{r}, t) = \frac{1}{Z_0}\mathrm{Re}\{E_0\ \exp[i(\mathbf{q}_p^s \cdot \mathbf{r} - \omega t)]\mathbf{h}(\mathbf{q}_p^s)\}, \tag{5}$$

where $Z_0 = \sqrt{\mu_0/\epsilon_0}$ is the wave impedance in vacuum and

$$\mathbf{h}(\mathbf{q}_p^s) = \frac{\mathbf{q}_p^s \times \hat{\mathbf{e}}(\mathbf{q}_p^s)}{\omega\mu Z_0}. \tag{6}$$

We now consider a planar interface between two different homogeneous, in general anisotropic, media: (1) on the left and (2) on the right of the interface. The interface is perpendicular to the z axis, which is directed from the left to right, at $z = 0$. Let us assume a plane electromagnetic wave of amplitude E_{in}, angular frequency ω, wave vector $\mathbf{q}_{p'}^{+(1)}$, and polarization eigenvector $\hat{\mathbf{e}}(\mathbf{q}_{p'}^{+(1)})$ incident on the interface from the left. Scattering at the interface gives rise to reflected and transmitted plane waves of wave vectors $\mathbf{q}_p^{-(1)}$ and $\mathbf{q}_p^{+(2)}$, $p = 1, 2$, respectively, characterized by the associated polarization eigenvectors. Time invariance and translation invariance parallel to the interface imply that ω and $\mathbf{q}_\parallel$ remain the same for all these waves, while linearity imposes that the corresponding amplitudes are proportional to E_{in}; we write them as $S_{pp'}^{-+}E_{\mathrm{in}}$ and $S_{pp'}^{++}E_{\mathrm{in}}$, respectively. Continuity of the tangential components of the wave field at the interface yields

$$\begin{pmatrix} -\hat{e}_x(\mathbf{q}_1^{-(1)}) & -\hat{e}_x(\mathbf{q}_2^{-(1)}) & \hat{e}_x(\mathbf{q}_1^{+(2)}) & \hat{e}_x(\mathbf{q}_2^{+(2)}) \\ -\hat{e}_y(\mathbf{q}_1^{-(1)}) & -\hat{e}_y(\mathbf{q}_2^{-(1)}) & \hat{e}_y(\mathbf{q}_1^{+(2)}) & \hat{e}_y(\mathbf{q}_2^{+(2)}) \\ -h_x(\mathbf{q}_1^{-(1)}) & -h_x(\mathbf{q}_2^{-(1)}) & h_x(\mathbf{q}_1^{+(2)}) & h_x(\mathbf{q}_2^{+(2)}) \\ -h_y(\mathbf{q}_1^{-(1)}) & -h_y(\mathbf{q}_2^{-(1)}) & h_y(\mathbf{q}_1^{+(2)}) & h_y(\mathbf{q}_2^{+(2)}) \end{pmatrix} \begin{pmatrix} S_{1p'}^{-+} \\ S_{2p'}^{-+} \\ S_{1p'}^{++} \\ S_{2p'}^{++} \end{pmatrix} = \begin{pmatrix} \hat{e}_x(\mathbf{q}_{p'}^{+(1)}) \\ \hat{e}_y(\mathbf{q}_{p'}^{+(1)}) \\ h_x(\mathbf{q}_{p'}^{+(1)}) \\ h_y(\mathbf{q}_{p'}^{+(1)}) \end{pmatrix}, \tag{7}$$

for $p' = 1, 2$. Similarly, for incidence on the interface from the right, we obtain the corresponding reflection and transmission amplitudes, $S_{pp'}^{+-}$ and $S_{pp'}^{--}$, respectively, from the linear system

$$\begin{pmatrix} -\hat{e}_x(\mathbf{q}_1^{-(1)}) & -\hat{e}_x(\mathbf{q}_2^{-(1)}) & \hat{e}_x(\mathbf{q}_1^{+(2)}) & \hat{e}_x(\mathbf{q}_2^{+(2)}) \\ -\hat{e}_y(\mathbf{q}_1^{-(1)}) & -\hat{e}_y(\mathbf{q}_2^{-(1)}) & \hat{e}_y(\mathbf{q}_1^{+(2)}) & \hat{e}_y(\mathbf{q}_2^{+(2)}) \\ -h_x(\mathbf{q}_1^{-(1)}) & -h_x(\mathbf{q}_2^{-(1)}) & h_x(\mathbf{q}_1^{+(2)}) & h_x(\mathbf{q}_2^{+(2)}) \\ -h_y(\mathbf{q}_1^{-(1)}) & -h_y(\mathbf{q}_2^{-(1)}) & h_y(\mathbf{q}_1^{+(2)}) & h_y(\mathbf{q}_2^{+(2)}) \end{pmatrix} \begin{pmatrix} S_{1p'}^{--} \\ S_{2p'}^{--} \\ S_{1p'}^{+-} \\ S_{2p'}^{+-} \end{pmatrix}$$

$$= -\begin{pmatrix} \hat{e}_x(\mathbf{q}_{p'}^{-(2)}) \\ \hat{e}_y(\mathbf{q}_{p'}^{-(2)}) \\ h_x(\mathbf{q}_{p'}^{-(2)}) \\ h_y(\mathbf{q}_{p'}^{-(2)}) \end{pmatrix}, \tag{8}$$

for $p' = 1, 2$. We note that the 4×4 matrices on the left-hand side of Eqs. (7) and (8) are identical, so a single lower–upper decomposition has to be performed prior to back substitution [47].

Since the LMS method is meant to deal with composite layered structures of photonic crystals, where an interface between two different homogeneous media constitutes a component of a unit slice, which in general contains, in addition, planes of particles of given two-dimensional periodicity, it is convenient to write the parallel component of the wave vector in the form $\mathbf{q}_\parallel = \mathbf{k}_\parallel + \mathbf{g}$, where $\mathbf{k}_\parallel$ is the reduced wave vector within the surface Brillouin zone and $\mathbf{g}$ is a certain reciprocal lattice vector, and then express the waves on the left (right) of the interface with respect to an origin at $-\mathbf{d}_l$ ($\mathbf{d}_r$) from the center. Referred to these origins, the reflection and transmission matrix elements of the interface, for given ω and $\mathbf{k}_\parallel$, become

$$\begin{aligned} Q^{\mathrm{I}}_{\mathbf{g}p,\mathbf{g}'p'} &= \delta_{\mathbf{g},\mathbf{g}'} S^{++}_{pp'} \exp[i(\mathbf{q}_p^{+(2)} \cdot \mathbf{d}_r + \mathbf{q}_{p'}^{+(1)} \cdot \mathbf{d}_l)], \\ Q^{\mathrm{II}}_{\mathbf{g}p,\mathbf{g}'p'} &= \delta_{\mathbf{g},\mathbf{g}'} S^{+-}_{pp'} \exp[i(\mathbf{q}_p^{+(2)} \cdot \mathbf{d}_r - \mathbf{q}_{p'}^{-(2)} \cdot \mathbf{d}_r)], \\ Q^{\mathrm{III}}_{\mathbf{g}p,\mathbf{g}'p'} &= \delta_{\mathbf{g},\mathbf{g}'} S^{-+}_{pp'} \exp[-i(\mathbf{q}_p^{-(1)} \cdot \mathbf{d}_l - \mathbf{q}_{p'}^{+(1)} \cdot \mathbf{d}_l)], \\ Q^{\mathrm{IV}}_{\mathbf{g}p,\mathbf{g}'p'} &= \delta_{\mathbf{g},\mathbf{g}'} S^{--}_{pp'} \exp[-i(\mathbf{q}_p^{-(1)} \cdot \mathbf{d}_l + \mathbf{q}_{p'}^{-(2)} \cdot \mathbf{d}_r)]. \end{aligned} \tag{9}$$

The reflection and transmission matrices for a multilayer slab are obtained from the corresponding matrices of the individual layers, in the manner described in Refs. [34–36].

3. RESULTS AND DISCUSSION

In the present paper, we report a comprehensive study of the MO response and compare the efficiency of different mechanisms to enhance the Faraday rotation angle in the case of a 100 nm thick Bi:YIG film patterned with a square array, with period a, of Ag nanodisks, of diameter 100 nm and height 50 nm, supported by a silica substrate. A DC magnetic field is applied perpendicular to the surface and is assumed to saturate the magnetization of the garnet film. A schematic of the structure under consideration is depicted in Fig. 1. We note that the nanoparticles that we consider here are symmetric under rotation in the $x - y$ plane, while the lattice is identical in the x and y directions. This configuration is chosen because, for normally incident light, the polarization modes are degenerate. Therefore, the polarization direction is immaterial while, at the same time, we expect efficient polarization conversion rates. The size of the particles is similar to those considered in previous studies [30,31].

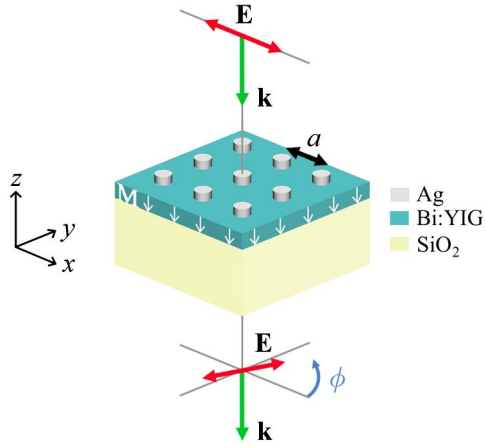

Fig. 1. Schematic of the structure under consideration: a square array of Ag nanodisks, of diameter 100 nm and height 50 nm, with lattice constant a, on top of a 100 nm thick Bi:YIG film supported by a SiO_2 substrate. The film is magnetically saturated by an external static magnetic field applied perpendicular to the surface. The structure is illuminated by normally incident light (Faraday configuration).

The optical parameters for Ag and Bi:YIG in the frequency region under consideration are obtained by interpolating to available experimental data [48,49], while for SiO_2 a constant refractive index $n = 1.46$ is assumed. Our calculations are carried out by both the LMS method, that we properly extended to structures comprising MO layers as described in Section 2, and the commercial finite-element solver implemented in the COMSOL Multiphysics package. Convergence was carefully checked in both methods. The results obtained by the two methods are in very good agreement, except at the resonances where the results are slightly different (the differences do not exceed 10%) as convergence in COMSOL calculations becomes prohibitively time-consuming. The convergence associated with the number of finite elements used in COMSOL was dramatically improved when we assumed cylindrical particles with slightly rounded corners. In this respect, it is worth noting that a structure similar to that which we consider here was modeled by COMSOL, assuming spherical particles to analyze the experimental spectra obtained for Au nanodisks [31]. On the contrary, the LMS method ensures fast convergence and accurate results for the actual particle shape if we truncate the relevant angular momentum expansions at $\ell_{\max} = 14$ and $\ell_{\mathrm{cut}} = 22$ [36] and use 145 two-dimensional reciprocal lattice vectors in the plane wave expansions of the wave field [34,35], being about two orders of magnitude faster than the finite-elements method.

A bare Bi:YIG film on a silica substrate supports guided modes, localized in the film. These modes cannot be excited by a normally incident wave as they lie outside the light cone and thus cannot match continuously a propagating mode of the EM field outside the film; momentum and energy cannot be simultaneously conserved. The presence of the periodic array of nanoparticles causes a folding of the guided modes within the surface Brillouin zone or, in other words, diffraction at the lattice provides the missing momentum, which allows coupling of normally incident light to the film modes. These modes are

mostly confined inside the Bi:YIG film, which is the high-index material. In common nonmagnetic high-index dielectric films, reflection symmetry with respect to a plane perpendicular to the film allows one to classify the guided modes into transverse magnetic (TM) or transverse electric (TE) if the magnetic or the electric field, respectively, oscillates parallel to the interfaces [50]. In our case though, the optical response of magnetic Bi:YIG is described by a permittivity tensor [49], which breaks the above symmetry. Thus, the modes cannot be categorized as purely TM or purely TE [51]. However, they still have a predominant TM or TE character and, if the film is coated with a periodic array of scatterers, they can be excited by externally incident light with the proper propagation direction and polarization state [52], leading to resonance dips in the corresponding transmission spectra, as shown in Fig. 2.

In Fig. 3(a), we display the transmittance of the structure under consideration, for a nanoparticle array of lattice constant $a = 310$ nm, illuminated by linearly polarized normally incident light, as calculated by both the LMS method (full line) and the finite-element method implemented in COMSOL (symbols). The excitation of hybrid LSP and waveguide modes of the garnet film are clearly manifested in the spectrum. More specifically, the spectrum exhibits two drops in the transmission, which are associated with strong Faraday rotation, while both LMS and COMSOL calculations deliver essentially the same spectra, with small differences of a few percent on resonance, as shown in Fig. 3(b). It is worth noting that the rotation angle is much larger than that induced by the bare Bi:YIG film without the metallic nanoparticles [see Fig. 3(c)]. The origin of these modes becomes evident, also, from the corresponding field profiles shown in Fig. 3. The longer-wavelength dip is due to the excitation of a hybrid mode with a mainly LSP character, while the shorter-wavelength dip arises from a predominantly TE-like guided film mode. Depending on the geometry of the structure, the interaction of LSP with film modes can give rise to hybrid modes with intriguing characteristics [40,52–55], which can be exploited for tailoring the Faraday effect.

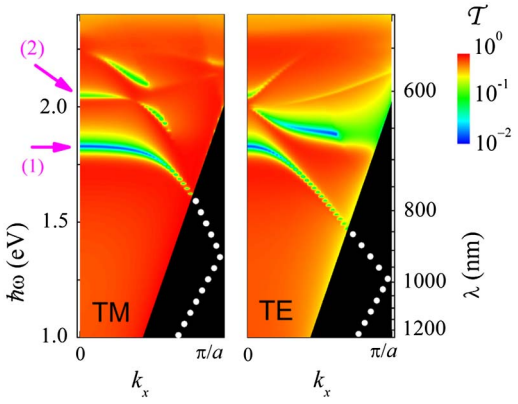

Fig. 2. Transmittance of TM- and TE-polarized light incident with a parallel component of the wave vector k_x on the structure of Fig. 1 with $a = 310$ nm. The dotted lines show the corresponding guided modes in the Bi:YIG film, which lie outside of the air light cone (black region). The arrows mark the (1) LSP and (2) TE-like film modes excited at normal incidence.

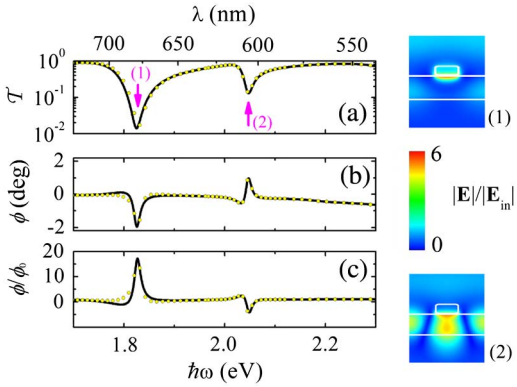

Fig. 3. (a) Transmission spectrum of the structure of Fig. 1 for $a = 310$ nm, at normal incidence, calculated by the LMS method (solid line) and by the finite-element method implemented in COMSOL (symbols). The relative (with respect to the incident field) electric field amplitude profiles at the resonances marked with arrows are shown in the margin. (b) Corresponding Faraday rotation angle. (c) Enhancement of the Faraday rotation angle ϕ with respect to that of the uncoated Bi:YIG film supported by the silica substrate ϕ_0.

Our results show that the hybrid mode close to $\lambda = 680$ nm, of predominant LSP character, is associated with a large Faraday rotation angle of −1.9°, which corresponds to a 17-fold enhancement compared to the uncoated Bi:YIG film, but transmission is strongly suppressed as low as 1.5%. On the other hand, the resonance due to the excitation of the film-like hybrid mode, at $\lambda = 606$ nm, yields a smaller rotation angle, of 1°, which is only ∼4 times larger in magnitude than the corresponding Faraday rotation angle induced by the bare Bi:YIG film but transmission is higher, reaching 14%. It is worth noting that the corresponding ellipticity angles at the above wavelengths are vanishingly small, which means that we obtain linearly polarized transmitted waves. Geometry can be optimized depending on the target wavelength while additional guided film modes can also be excited. In Fig. 4, we depict the systematic evolution of the spectra as we vary the lattice constant of the nanoparticle array, obtained by means of large-scale LMS calculations. By increasing the lattice constant, the surface Brillouin zone shrinks and, consequently, the folded

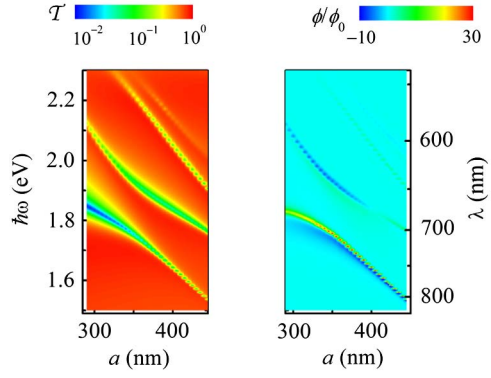

Fig. 4. Spectral variation of the transmittance and Faraday rotation angle enhancement, for light incident normally on the structure of Fig. 1, as a function of the lattice parameter a.

bands of quasi-guided film modes at the center of the Brillouin zone move lower in frequency, while higher modes of this type, e.g., TM-like, also appear within the spectral window under consideration. On the other hand, the positions of the LSP modes are rather insensitive to the lattice spacing. Interactions between the different modes, which are stronger when the modes are close in frequency and have significant overlap in space, lead to the formation of modes of hybrid character that manifest themselves as resonance dips in the corresponding transmission spectra, as can be seen in Fig. 4. The associated Faraday rotation angle increases, compared to the uncoated Bi:YIG film, as a result of the strong localization of the wave field in the active magnetic region, depending on the specific field distribution.

As mentioned already, there is a trade-off between the transmittance and the Faraday rotation angle, which led to the introduction of a figure of merit defined as FOM $= \sqrt{\mathcal{T}}|\phi|$ [17,28,29]. Our systematic calculations show that FOM can be optimized by properly adjusting the geometrical parameters involved for any targeted wavelength in the visible and infrared parts of the spectrum. For example, in Fig. 5, we display the results obtained for a lattice constant $a = 350$ nm, which show a maximum Faraday rotation angle of −2.38° with transmittance 2.2% (FOM = 0.35) at $\lambda = 706$ nm. The ellipticity angle, η, displayed in Fig. 5(b) with a dotted line, vanishes at the peak position. Interestingly, around $\lambda = 650$ nm, we can see another maximum of FOM, which does not correspond to a minimum transmittance. In this region, the ellipticity angle crosses zero at two wavelengths: at $\lambda = 653$ nm with $\phi = -0.35°$ and $\mathcal{T} = 78\%$ (FOM = 0.31) and at $\lambda = 642$ nm with $\phi = 0.74°$ and $\mathcal{T} = 6.3\%$ (FOM = 0.19). As shown in Fig. 5(c), increased FOM also appears at shorter wavelengths, at about $\lambda = 550$ nm, due to the stronger MO response of Bi:YIG at these wavelengths, which, however, is accompanied by an increase in the ellipticity angle. Increasing the lattice constant to $a = 442$ nm, the low-frequency resonance moves to the infrared and, according to our calculations (see Fig. 4), a 29-fold enhancement of the Faraday rotation angle that reaches −1.2° at $\lambda = 803$ nm with a practically vanishing ellipticity angle is induced. At the same time, the transmittance drops compared to that of the uncoated Bi:YIG film from 66% to 10%. It should be noted that in the infrared spectrum, high values of the Faraday rotation angle combined with significant transmission have been reported in the literature utilizing the effect of extraordinary optical transmission [27]. However, recent attempts to take advantage of this effect at visible frequencies resulted in a maximum figure of merit of only 0.24 for the same (100 nm) Bi:YIG film thickness [28]. Increasing the thickness of the Bi:YIG film enables the appearance of higher-order slab modes, leading to increased Faraday angles and transmittance, which translates to a higher FOM [24]. However, this FOM enhancement relative to the bare garnet film is not as high as the other cases considered here.

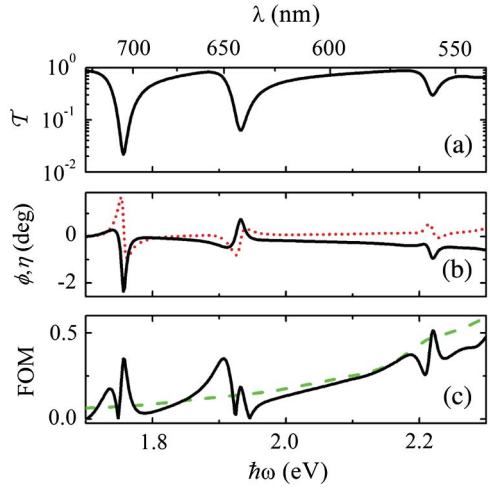

Fig. 5. (a) Transmission spectrum at normal incidence for the structure of Fig. 1 with $a = 350$ nm. (b) Corresponding Faraday rotation angle ϕ (solid line) and ellipticity angle η (dotted line). (c) Corresponding figure of merit (solid line), together with the figure of merit of the uncoated Bi:YIG film supported by the silica substrate (dashed line).

4. CONCLUSIONS

In summary, the LMS method was extended to treat structures comprising homogeneous layers of MO materials, such as that studied in the present work, and constitutes a powerful computational tool for fast and accurate full electrodynamic calculations, enabling physical insight. By means of large-scale systematic calculations, using this method, we reported a thorough study of the Faraday effect in a thin magnetic Bi:YIG film coated with a square array of Ag nanodisks on a silica substrate. Our results provide evidence that significant enhancement of the Faraday rotation angle can be achieved, although with a cost in the transmittance, due to the strong localization of light in the magnetic film associated with hybrid particle plasmon-film quasi-guided modes. After explaining the underlying physics to a degree that goes beyond existing interpretation, we show that, by optimizing the geometric parameters involved, the figure of merit can be increased by more than one order of magnitude, compared to the uncoated film, in selected regions of frequency. High performance, ultrathin size, polarization insensitivity, and frequency tunability render this structure very promising for nanophotonic applications.

Funding. IKY Fellowships of Excellence for Postgraduate Studies in Greece–Siemens Program.

Acknowledgment. Dr. Evangelos Almpanis gratefully acknowledges funding from "IKY Fellowships of Excellence for Postgraduate Studies in Greece–SIEMENS Program." Fruitful discussions with Dr. Aristi Christofi about computational issues are also acknowledged. The authors gratefully thank Marianna Dionysopoulou for her artistic support in the graphical illustrations.

REFERENCES

1. M. Zamani, M. Ghanaatshoar, and H. Alisafaee, "Adjustable magneto-optical isolators with high transmittance and large Faraday rotation," J. Opt. Soc. Am. B **28**, 2637–2642 (2011).

2. K. Fang, Z. Yu, V. Liu, and S. Fan, "Ultracompact nonreciprocal optical isolator based on guided resonance in a magneto-optical photonic crystal slab," Opt. Lett. **36**, 4254–4256 (2011).
3. H. Kato, T. Matsushita, A. Takayama, M. Egawa, K. Nishimura, and M. Inoue, "Theoretical analysis of optical and magneto-optical properties of one-dimensional magnetophotonic crystals," J. Appl. Phys. **93**, 3906–3911 (2003).
4. M. Liu and X. Zhang, "Plasmon-boosted magneto-optics," Nat. Photonics **7**, 429–430 (2013).
5. G. Armelles, A. Cebollada, A. García-Martín, and M. U. González, "Magnetoplasmonics: combining magnetic and plasmonic functionalities," Adv. Opt. Mater. **1**, 10–35 (2013).
6. I. S. Maksymov, "Magneto-plasmonics and resonant interaction of light with dynamic magnetisation in metallic and all-magneto-dielectric nanostructures," Nanomaterials **5**, 577–613 (2015).
7. S. A. Maier, *Plasmonics: Fundamentals and Applications* (Springer, 2007).
8. F. E. Moolekamp and K. L. Stokes, "Magnetooptical response of gold-magnetite nanocomposite films," IEEE Trans. Magn. **45**, 4888–4891 (2009).
9. P. K. Jain, Y. Xiao, R. Walsworth, and A. E. Cohen, "Surface plasmon resonance enhanced magneto-optics (SuPREMO): Faraday rotation enhancement in gold-coated iron oxide nanocrystals," Nano Lett. **9**, 1644–1650 (2009).
10. B. Sepúlveda, J. B. González-Díaz, A. García-Martín, L. M. Lechuga, and G. Armelles, "Plasmon-induced magneto-optical activity in nanosized gold disks," Phys. Rev. Lett. **104**, 147401 (2010).
11. R. K. Dani, H. Wanh, S. H. Bossmann, G. Wysin, and V. Chikan, "Faraday rotation enhancement of gold coated Fe_2O_3 nanoparticles: comparison of experiment and theory," J. Chem. Phys. **135**, 224502 (2011).
12. G. Armelles, A. Cebollada, A. García-Martín, J. M. Montero-Moreno, M. Waleczek, and K. Nielsch, "Magneto-optical properties of core-shell magneto-plasmonic Au–$Co_xFe_{3-x}O_4$ nanowires," Langmuir **28**, 9127–9130 (2012).
13. M. Caminale, L. Anghinolfi, E. Magnano, F. Bondino, M. Canepa, L. Mattera, and F. Bisio, "Tuning the magneto-optical response of iron oxide nanocrystals in Au- and Ag-based plasmonic media," ACS Appl. Mater. Interface **5**, 1955–1960 (2013).
14. V. Yannopapas, "Magnetochirality in hierarchical magnetoplasmonic clusters," Solid State Commun. **217**, 47–52 (2015).
15. V. Yannopapas and A. G. Vanakaras, "Strong magnetochiral dichroism in suspensions of magnetoplasmonic nanohelices," ACS Photon. **2**, 1030–1038 (2015).
16. A. B. Khanikaev, S. H. Mousavi, G. Shvets, and Y. S. Kivshar, "One-way extraordinary optical transmission and nonreciprocal spoof plasmons," Phys. Rev. Lett. **105**, 126804 (2010).
17. A. B. Khanikaev, A. V. Baryshev, A. A. Fedyanin, A. B. Granovsky, and M. Inoue, "Anomalous Faraday effect of a system with extraordinary optical transmittance," Opt. Express **15**, 6612–6622 (2007).
18. S. Chen, F. Fan, X. He, M. Chen, and S. Chang, "Multifunctional magneto-metasurface for terahertz one-way transmission and magnetic field sensing," Appl. Opt. **54**, 9177–9182 (2015).
19. V. I. Belotelov, I. A. Akimov, M. Pohl, V. A. Kotov, S. Kasture, A. S. Vengurlekar, A. V. Gopal, D. R. Yakovlev, A. K. Zvezdin, and M. Bayer, "Enhanced magneto-optical effects in magneto-plasmonic crystals," Nat. Nanotechnol. **6**, 370–376 (2011).
20. A. V. Chetvertukhin, A. I. Musorin, T. V. Dolgova, H. Uchida, M. Inoue, and A. A. Fedyanin, "Transverse magneto-optical Kerr effect in 2D gold–garnet nanogratings," J. Magn. Magn. Mater. **383**, 110–113 (2015).
21. V. I. Belotelov, L. L. Doskolovich, and A. K. Zvezdin, "Extraordinary magneto-optical effects and transmission through metal-dielectric plasmonic systems," Phys. Rev. Lett. **98**, 077401 (2007).
22. M. Kataja, T. K. Hakala, A. Julku, M. J. Huttunen, S. van Dijken, and P. Törmä, "Surface lattice resonances and magneto-optical response in magnetic nanoparticle arrays," Nat. Commun. **6**, 7072 (2015).
23. D. Floess, T. Weiss, S. Tikhodeev, and H. Giessen, "Lorentz nonreciprocal model for hybrid magnetoplasmonics," Phys. Rev. Lett. **117**, 063901 (2016).
24. V. I. Belotelov, L. L. Doskolovich, V. A. Kotov, E. A. Bezus, D. A. Bykov, and A. K. Zvezdin, "Magnetooptical effects in the metal–dielectric gratings," Opt. Commun. **278**, 104–109 (2007).
25. V. I. Belotelov, L. L. Doskolovich, V. A. Kotov, and A. K. Zvezdin, "Magnetooptical properties of perforated metallic films," J. Magn. Magn. Mater. **310**, e843–e845 (2007).
26. D. Li, C. Lei, L. Chen, Z. Tang, S. Zhang, S. Tang, and Y. Du, "Waveguide plasmon resonance induced enhancement of the magneto-optics in a Ag/Bi:YIG bilayer structure," J. Opt. Soc. Am. B **32**, 2003–2008 (2015).
27. V. Dmitriev, F. Paixáo, and M. Kawakatsu, "Enhancement of Faraday and Kerr rotations in three-layer heterostructure with extraordinary optical transmission effect," Opt. Lett. **38**, 1052–1054 (2013).
28. C. Lei, L. Chen, Z. Tang, D. Li, Z. Cheng, S. Tang, and Y. Du, "Enhancement of magneto-optical Faraday effects and extraordinary optical transmission in a tri-layer structure with rectangular annular arrays," Opt. Lett. **41**, 729–732 (2016).
29. D. Li, L. Chen, C. Lei, J. L. Menendez, C. Mallada, Z. Tang, S. Tang, and Y. Du, "Plasmon-enhanced magneto-optical activity in a nanostructure with circle annular arrays," J. Opt. Soc. Am. B **33**, 922–927 (2016).
30. A. V. Baryshev, H. Uchida, and M. Inoue, "Peculiarities of plasmon-modified magneto-optical response of gold-garnet structures," J. Opt. Soc. Am. B **30**, 2371–2376 (2013).
31. A. V. Baryshev and A. M. Merzlikin, "Tunable plasmonic thin magneto-optical wave plate," J. Opt. Soc. Am. B **33**, 1399–1405 (2016).
32. J. Y. Chin, T. Steinle, T. Wehlus, D. Dregely, T. Weiss, V. I. Belotelov, B. Stritzker, and H. Giessen, "Nonreciprocal plasmonics enables giant enhancement of thin-film Faraday rotation," Nat. Commun. **4**, 1599 (2013).
33. D. Floess, J. Y. Chin, A. Kawatani, D. Dregely, H.-U. Habermeier, T. Weiss, and H. Giessen, "Tunable and switchable polarization rotation with non-reciprocal plasmonic thin films at designated wavelengths," Light Sci. Appl. **4**, e284 (2015).
34. N. Stefanou, V. Yannopapas, and A. Modinos, "Heterostructures of photonic crystals: frequency bands and transmission coefficients," Comput. Phys. Commun. **113**, 49–77 (1998).
35. N. Stefanou, V. Yannopapas, and A. Modinos, "MULTEM 2: a new version of the program for transmission and band-structure calculations of photonic crystals," Comput. Phys. Commun. **132**, 189–196 (2000).
36. G. Gantzounis and N. Stefanou, "Layer-multiple-scattering method for photonic crystals of nonspherical particles," Phys. Rev. **73**, 035115 (2006).
37. A. Christofi and N. Stefanou, "Layer multiple scattering calculations for nonreciprocal photonic structures," Int. J. Mod. Phys. B **28**, 1441012 (2014).
38. A. Christofi, N. Stefanou, and N. Papanikolaou, "Periodic structures of magnetic garnet particles for strong Faraday rotation enhancement," Phys. Rev. B **89**, 214410 (2014).
39. P. Varytis, P. A. Pantazopoulos, and N. Stefanou, "Enhanced Faraday rotation by crystals of core–shell magnetoplasmonic nanoparticles," Phys. Rev. B **93**, 214423 (2016).
40. E. Almpanis and N. Papanikolaou, "Comparison of Ag and Si nanoparticle arrays: mimicking subwavelength plasmonic field concentrations with dielectric components," J. Opt. Soc. Am. B **33**, 99–104 (2016).
41. A. García-Martín, G. Armelles, and S. Pereira, "Light transport in photonic crystals composed of magneto-optically active materials," Phys. Rev. B **71**, 205116 (2005).
42. B. Caballero, A. García-Martín, and J. C. Cuevas, "Generalized scattering-matrix approach for magneto-optics in periodically patterned multilayer systems," Phys. Rev. B **85**, 245103 (2012).
43. V. I. Belotelov, D. A. Bykov, L. L. Doskolovich, A. N. Kalish, and A. K. Zvezdin, "Extraordinary transmission and giant magneto-optical transverse Kerr effect in plasmonic nanostructured films," J. Opt. Soc. Am. B **26**, 1594–1598 (2009).
44. P. Yeh, "Electromagnetic propagation in birefringent layered media," J. Opt. Soc. Am. **69**, 742–756 (1979).
45. F. Tisseur and K. Meerbergen, "The quadratic eigenvalue problem," SIAM Rev. **43**, 235–286 (2001).

46. S. Hammarling, C. J. Munro, and F. Tisseur, "An algorithm for the complete solution of quadratic eigenvalue problems," ACM Trans. Math. Softw. **39**, 1–19 (2013).
47. W. H. Press, S. A. Teukolsky, W. T. Vetterling, and B. P. Flannery, *Numerical Recipes: The Art of Scientific Computing* (Cambridge University, 2007).
48. B. Johnson and R. W. Christy, "Optical constants of the noble metals," Phys. Rev. B **6**, 4370–4379 (1972).
49. V. Doormann, J.-P. Krumme, and H. Lenz, "Optical and magnetooptical tensor spectra of bismuth substituted yttrium iron garnet films," J. Appl. Phys. **68**, 3544–3553 (1990).
50. T. Ochiai and K. Sakoda, "Dispersion relation and optical transmittance of a hexagonal photonic crystal slab," Phys. Rev. B **63**, 125107 (2001).
51. M. S. Kushwaha and P. Halevi, "Magnetoplasmons in thin films in the perpendicular configuration," Phys. Rev. B **38**, 12428–12435 (1988).
52. G. Gantzounis, N. Stefanou, and V. Yannopapas, "Optical properties of a periodic monolayer of metallic nanospheres on a dielectric waveguide," J. Phys. **17**, 1791–1802 (2005).
53. V. Yannopapas, "Periodic arrays of film-coupled cubic nanoantennas as tunable plasmonic metasurfaces," Photonics **2**, 270–278 (2015).
54. E. Almpanis and N. Papanikolaou, "Designing photonic structures of nanosphere arrays on reflectors for total absorption," J. Appl. Phys. **114**, 083106 (2013).
55. E. Almpanis and N. Papanikolaou, "Dielectric nanopatterned surfaces for subwavelength light localization and sensing applications," Microelectron. Eng. **159**, 60–63 (2016).